**Supporting Information**

# Preparation of gas phase naked silver cluster cations outside a mass spectrometer from ligand protected clusters in solution

Madhuri Jash,[a] Arthur C. Reber,[b] Atanu Ghosh,[a] Depanjan Sarkar,[a] Mohammad Bodiuzzaman,[a] Pallab Basuri,[a] Ananya Baksi,[a] Shiv N. Khanna,*[b] and Thalappil Pradeep*[a]

[a]DST Unit of Nanoscience (DST UNS) and Thematic Unit of Excellence (TUE), Department of Chemistry, Indian Institute of Technology Madras, Chennai 600 036, India

[b]Department of Physics, Virginia Commonwealth University, Richmond, Virginia 23284, United States

*To whom correspondence should be addressed. E-mail: pradeep@iitm.ac.in; snkhanna@vcu.edu

## Table of Contents

## Supporting information 1

## Photograph of the instrumental set-up:

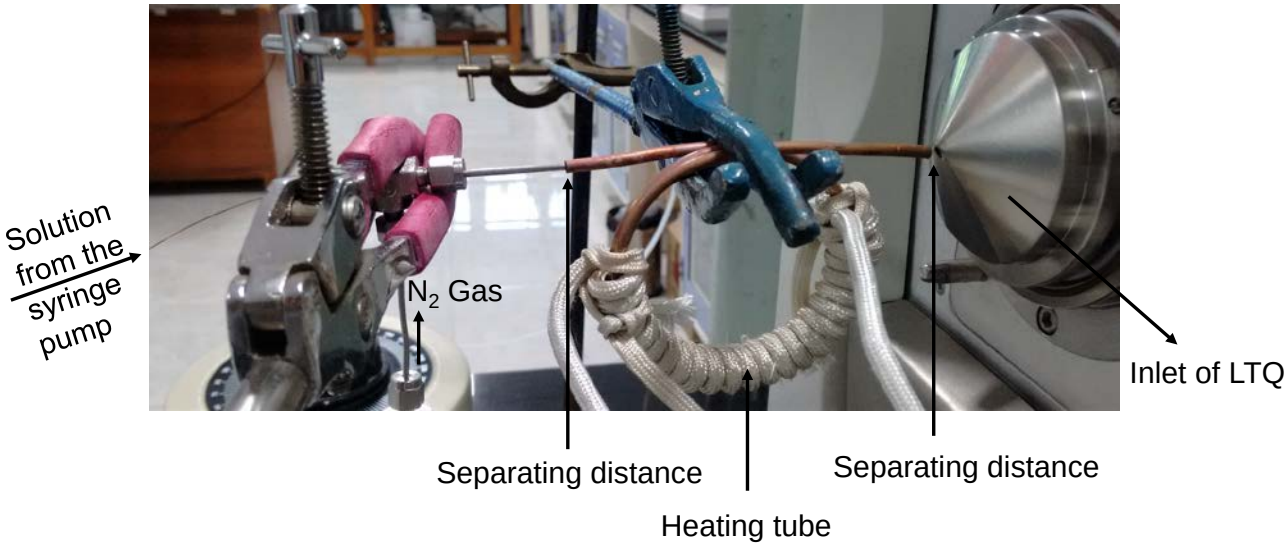


**S1:** Photograph of the instrumental set-up used for the creation of naked cluster ions.

## Supporting information 2

## Characterization of $[Ag_{18}H_{16}(TPP)_{10}]^{2+}$ cluster:

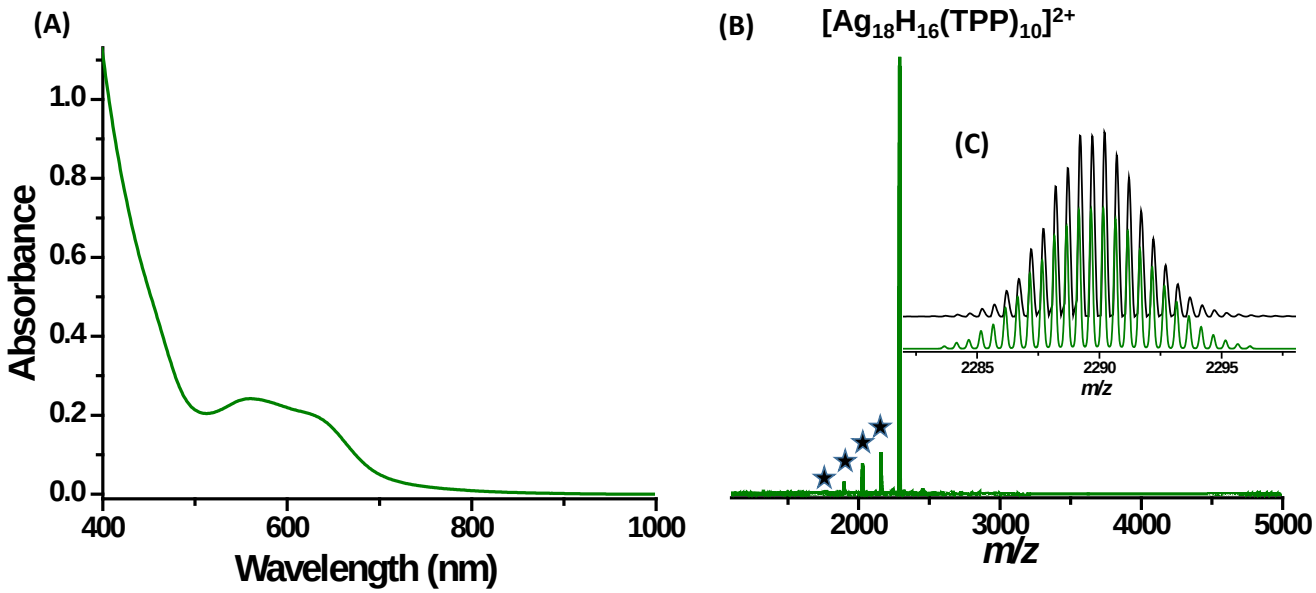


**Fig. S2** (A) UV-vis absorption spectrum of $[Ag_{18}H_{16}(TPP)_{10}]^{2+}$ cluster in MeOH showing characteristic absorption features. (B) ESI mass spectrum of the cluster in positive mode (using the G2-Si) is showing a sharp peak at m/z 2290 which is assigned as $[Ag_{18}H_{16}(TPP)_{10}]^{2+}$. Other small peaks separated by m/z 131 are due to $PPh_3$ loss which are shown by asterisks. (C) Peak at m/z 2290 is expanded, which is matching well with the calculated isotope pattern of $[Ag_{18}H_{16}(TPP)_{10}]^{2+}$.

**Supporting information 3**

## Characterization of $[Ag_{18}D_{16}(TPP)_{10}]^{2+}$ cluster:

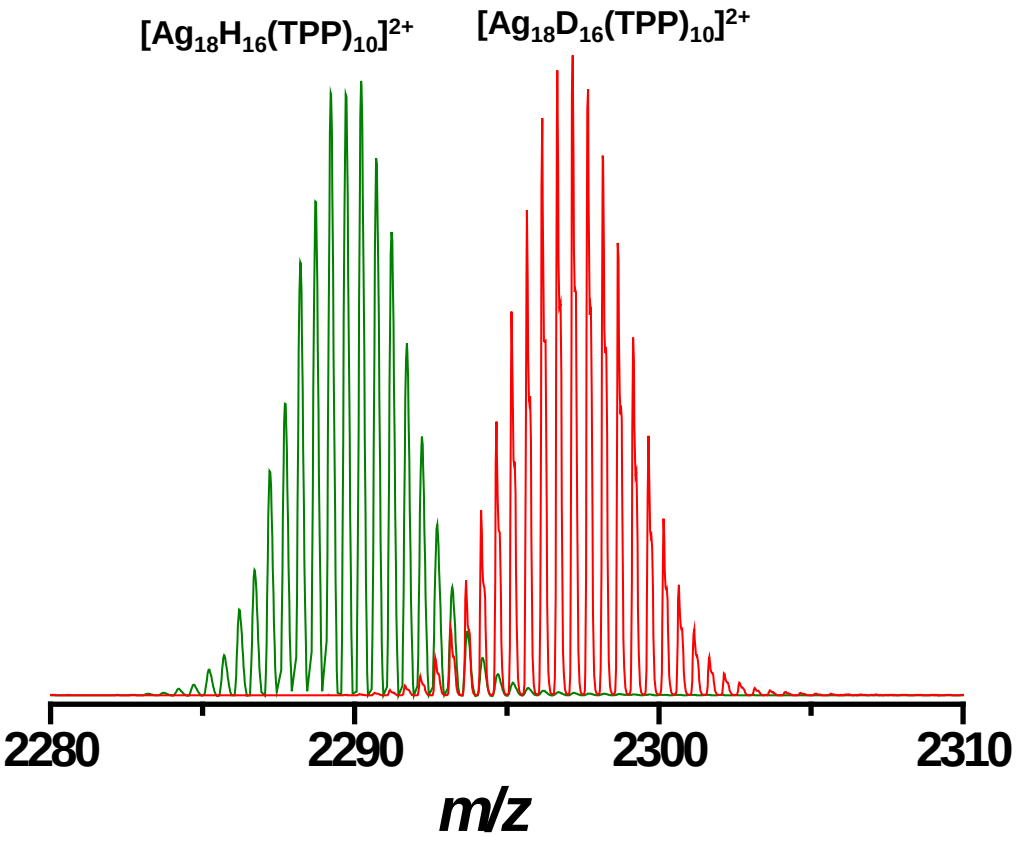


**Fig. S3** ESI mass spectra of $[Ag_{18}H_{16}(TPP)_{10}]^{2+}$ and $[Ag_{18}D_{16}(TPP)_{10}]^{2+}$ cluster ions (using the G2-Si). The mass shift is due to the exchange of hydride ions with deuteride ions. In $[Ag_{18}D_{16}(TPP)_{10}]^{2+}$, 100% exchange of hydrogen with deuterium was not there due to the presence of non-deutereted solvents in the synthesis.

**Supporting information 4**

**Comparison between the experimental and the calculated spectra:**

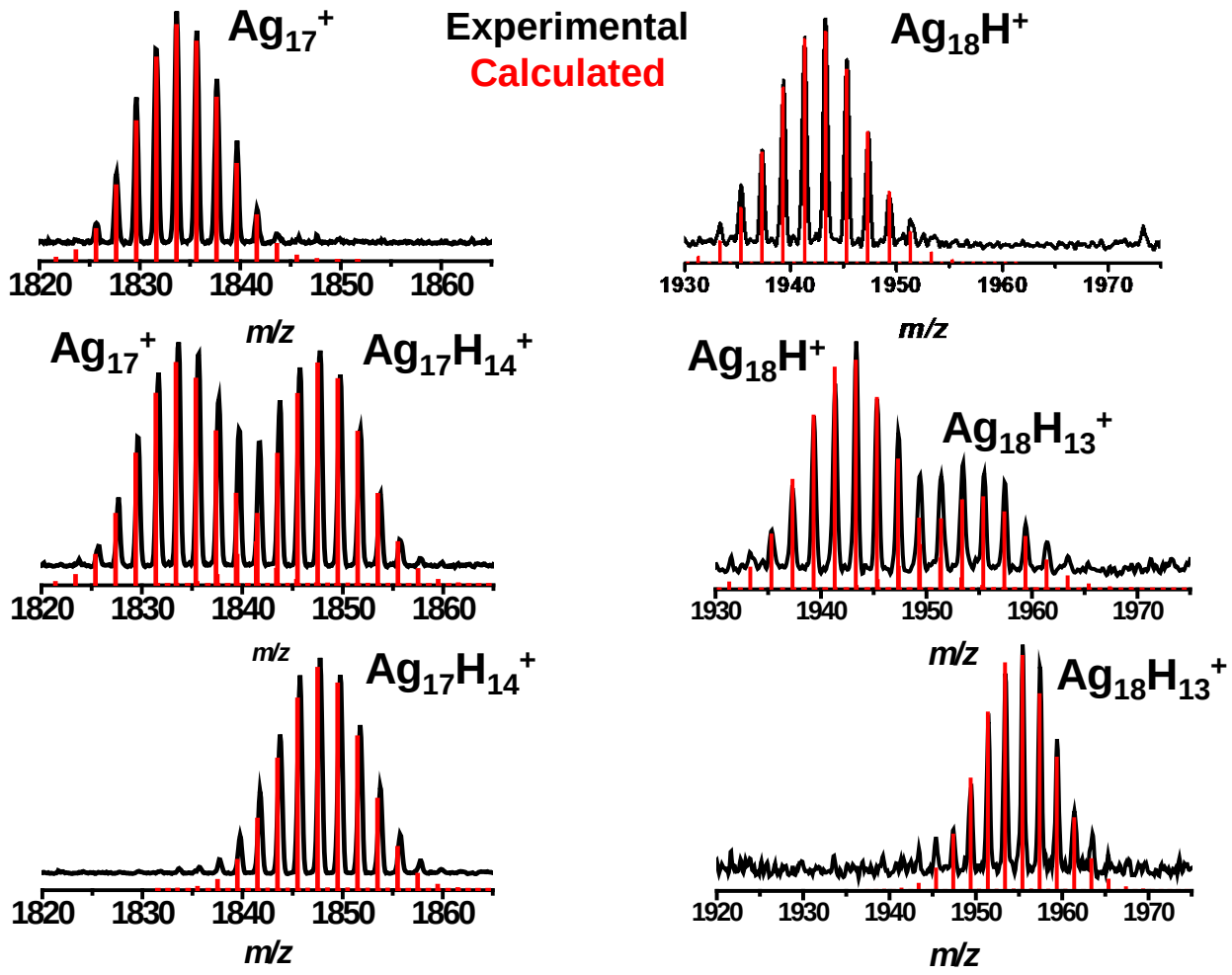


**Fig. S4** Experimental mass spectra of $Ag_{17}H_{14}^{+}$, $Ag_{17}^{+}$, $Ag_{18}H_{13}^{+}$ and $Ag_{18}H^{+}$ ions match well with the calculated isotopic patterns.

## Supporting information 5

## Full range ESI mass spectra of $[Ag_{18}H_{16}(TPP)_{10}]^{2+}$ cluster during heating:

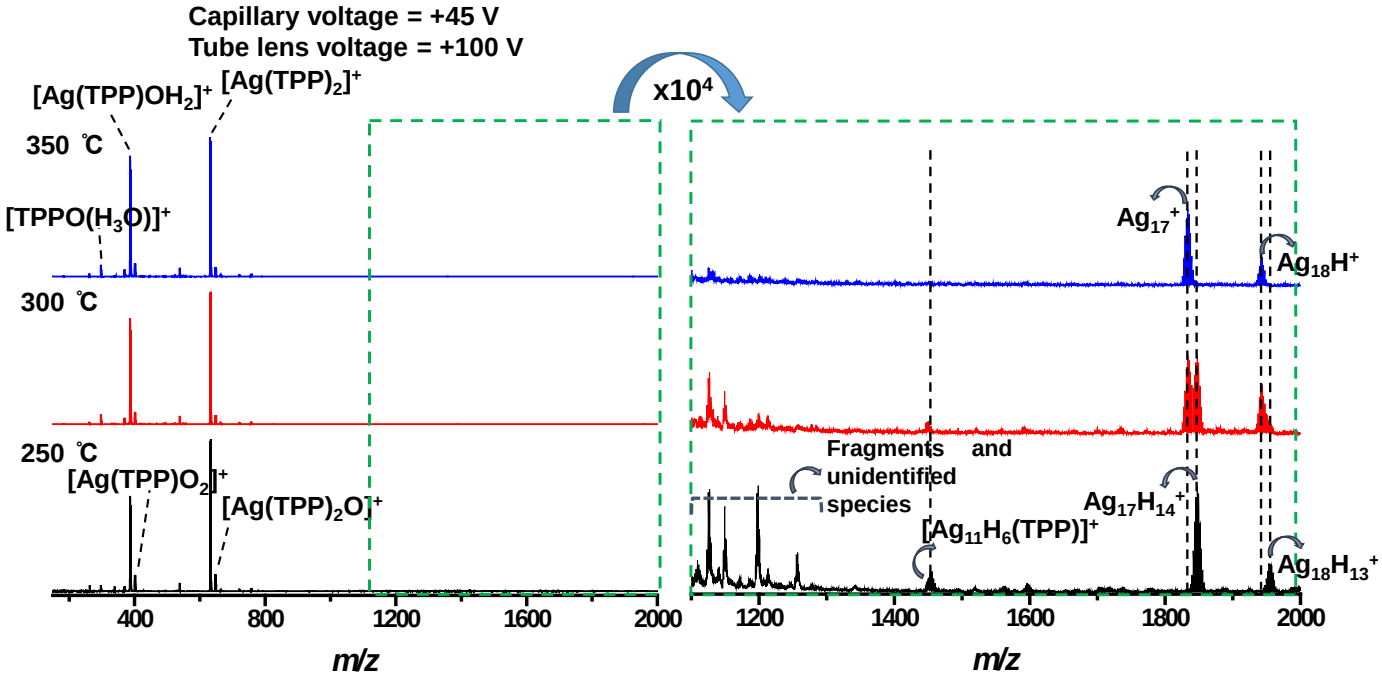


**Fig. S5** Full range ESI mass spectra of $[Ag_{18}H_{16}(TPP)_{10}]^{2+}$ cluster with varying the heating tube temperature from 250 ℃ to 350℃ at CV and TV of 45 V and 100 V, respectively. At 250℃, $Ag_{17}H_{14}^{+}$ and $Ag_{18}H_{13}^{+}$ were detected and at 300℃, $Ag_{17}^{+}$ and $Ag_{18}H^{+}$ were seen along with their hydride clusters. Finally, at 350℃ only $Ag_{17}^{+}$ and $Ag_{18}H^{+}$ were seen without mass selection. At lower mass region, there were oxidation peaks of $[Ag(TPP)]^{+}$, $[Ag(TPP)_2]^{+}$ and $TPP^{+}$.

## Supporting information 6

## Formation of $Ag_{17}^{+}$ from both $Ag_{17}H_{14}^{+}$ and $Ag_{17}D_{14}^{+}$:

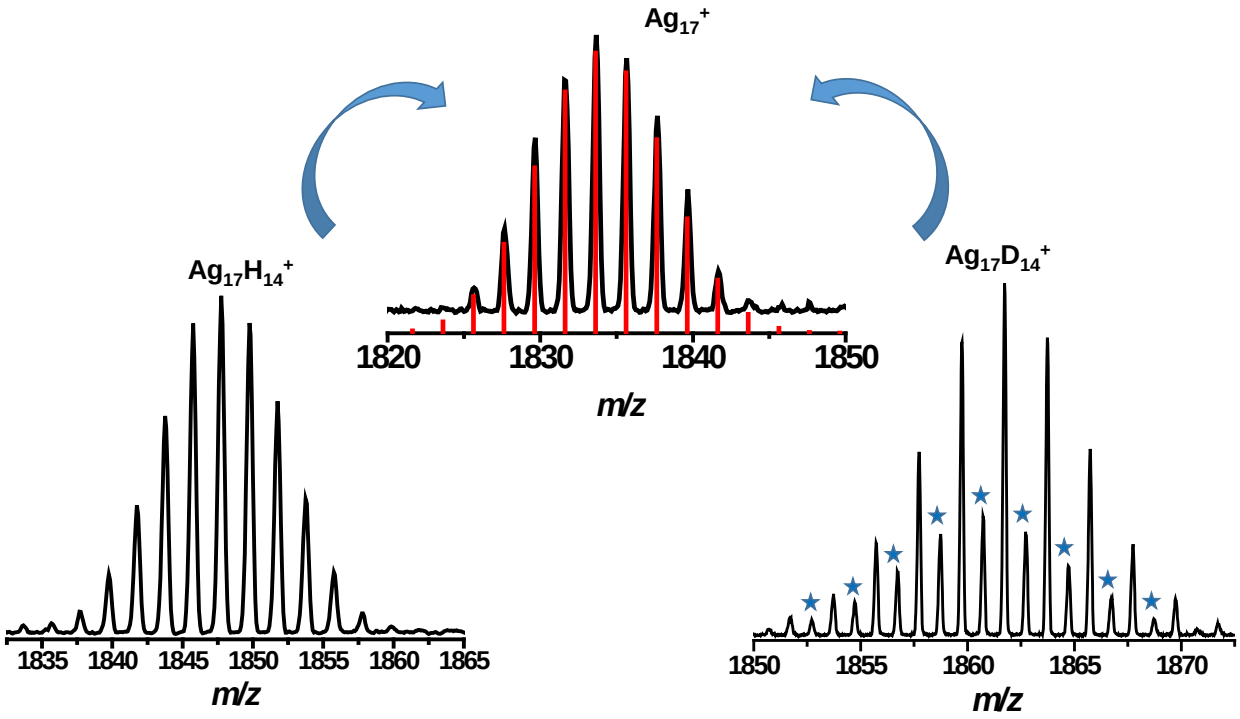


**Fig. S6** ESI mass spectra of $Ag_{17}H_{14}^{+}$ and $Ag_{17}D_{14}^{+}$ starting from $[Ag_{18}H_{16}(TPP)_{10}]^{2+}$ and $[Ag_{18}D_{16}(TPP)_{10}]^{2+}$, respectively. In the spectrum of $Ag_{17}D_{14}^{+}$, the peaks shown by asterisks (35%) are arising due to the presence of hydrogen, which are coming due to the partial isotope exchange (principally due to $Ag_{17}D_{13}H^{+}$), due to the presence of non-deuterated solvents. $Ag_{17}H_{14}^{+}$ and $Ag_{17}D_{14}^{+}$ are both converted to $Ag_{17}^{+}$ at 350℃.

## Supporting information 7

## Comparision of ESI mass spectra of $[Ag_{18}H_{16}(TPP)_{10}]^{2+}$ cluster during heating at different capillary and tube lens voltage:

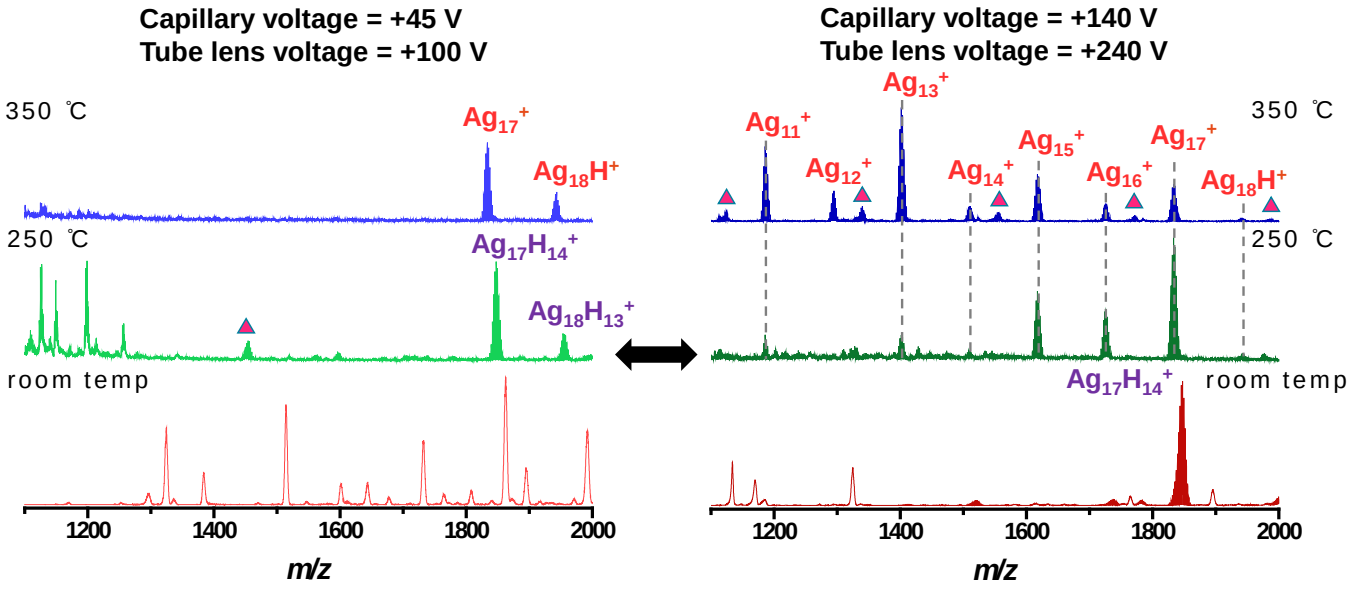


**Fig. S7** ESI mass spectra of $[Ag_{18}H_{16}(TPP)_{10}]^{2+}$ cluster with varying the heating tube temperature at CV and TV of 45 V and 100 V (left) and 140 V and 240 V (right). These two sets of CV and TV give different results at different temperatures of heating tube which is mainly due to the in-source fragmentation at higher CV and TV. Finally at 350℃, at CV and TV of 45 V and 100 V, only $Ag_{17}^{+}$ and $Ag_{18}H^{+}$ were seen without mass selection, whereas at CV and TV of 140 V and 240 V, naked clusters along with smaller core sizes appear due to fragmentation. The weak features shown by pink triangles are due to $[Ag_x(TPP)_y]^{+}$ clusters. Note the difference in intensities of odd and even numbered clusters.

**Supporting information 8**

**Full range ESI mass spectra of $[Ag_{18}H_{16}(TPP)_{10}]^{2+}$ cluster during heating at higher capillary and tube lens voltage:**

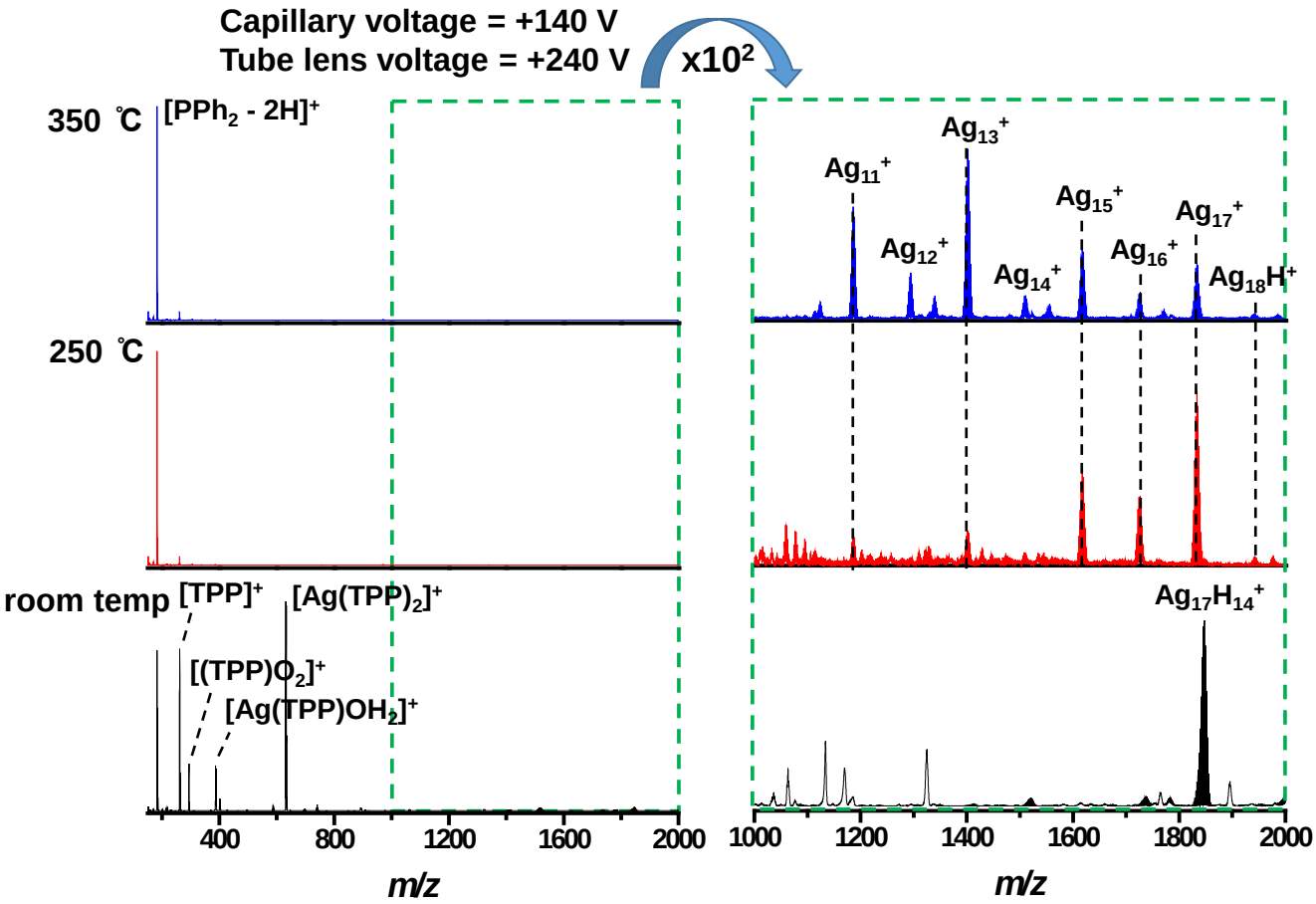


**Fig. S8** Full range ESI mass spectra of $[Ag_{18}H_{16}(TPP)_{10}]^{2+}$ cluster with varying heating tube temperature from room temperature to 350℃ at CV and TV of 140 V and 240V. At room temperature, $Ag_{17}H_{14}^{+}$ was detected along with some low mass region peaks. At 250℃, $Ag_{11}^{+}$, $Ag_{13}^{+}$, $Ag_{15}^{+}$, $Ag_{16}^{+}$, $Ag_{17}^{+}$ and $Ag_{18}H^{+}$ were seen. Finally at 350℃, all the naked clusters of silver along with $Ag_{17}^{+}$ and $Ag_{18}H^{+}$ were detected.

**Supporting information 9**

**Ion chronograms of selected ions:**

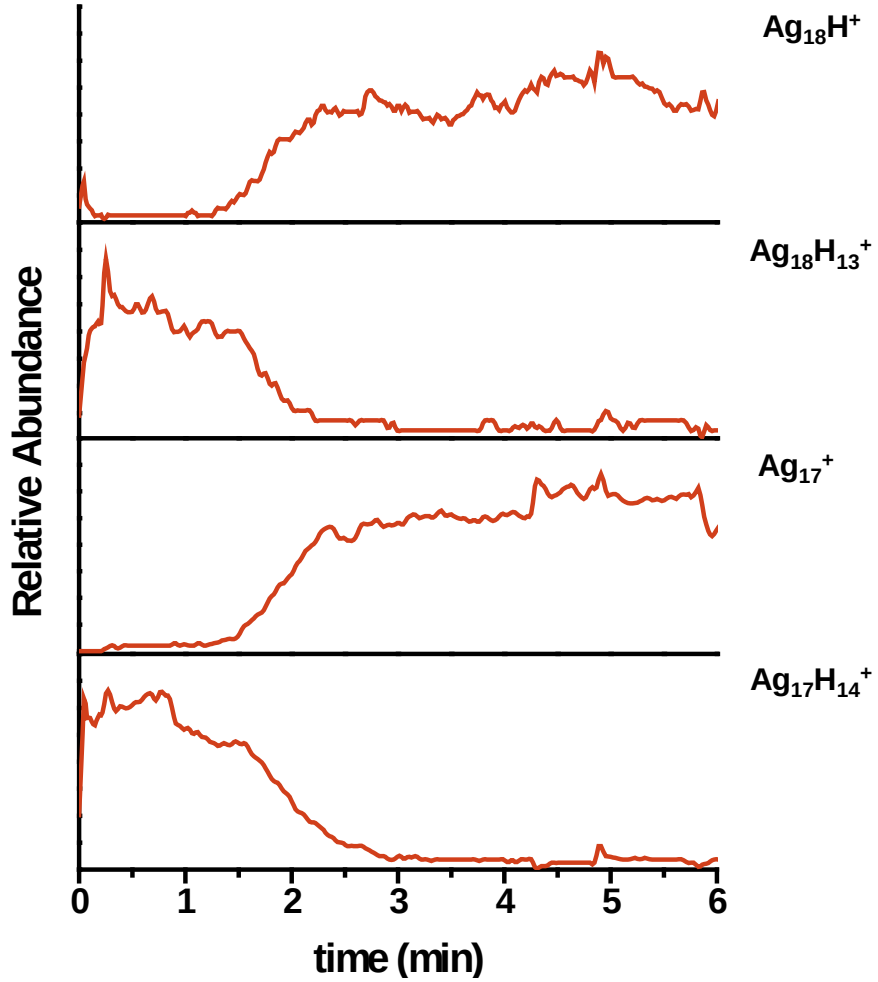


**Fig. S9** Ion chronograms of selected ions during the formation of naked clusters. At time zero the temperature was 250℃ and there were only existence of $Ag_{17}H_{14}^{+}$ and $Ag_{18}H_{13}^{+}$. Then slowly temperature was raised to 350℃ over a few minutes, which results the appearance of $Ag_{17}^{+}$ and $Ag_{18}H^{+}$.

## Supporting information 10

## $MS^2$ for $Ag_{17}^+$, $Ag_{17}H_{14}^+$ and $Ag_{18}H^+$ ions:

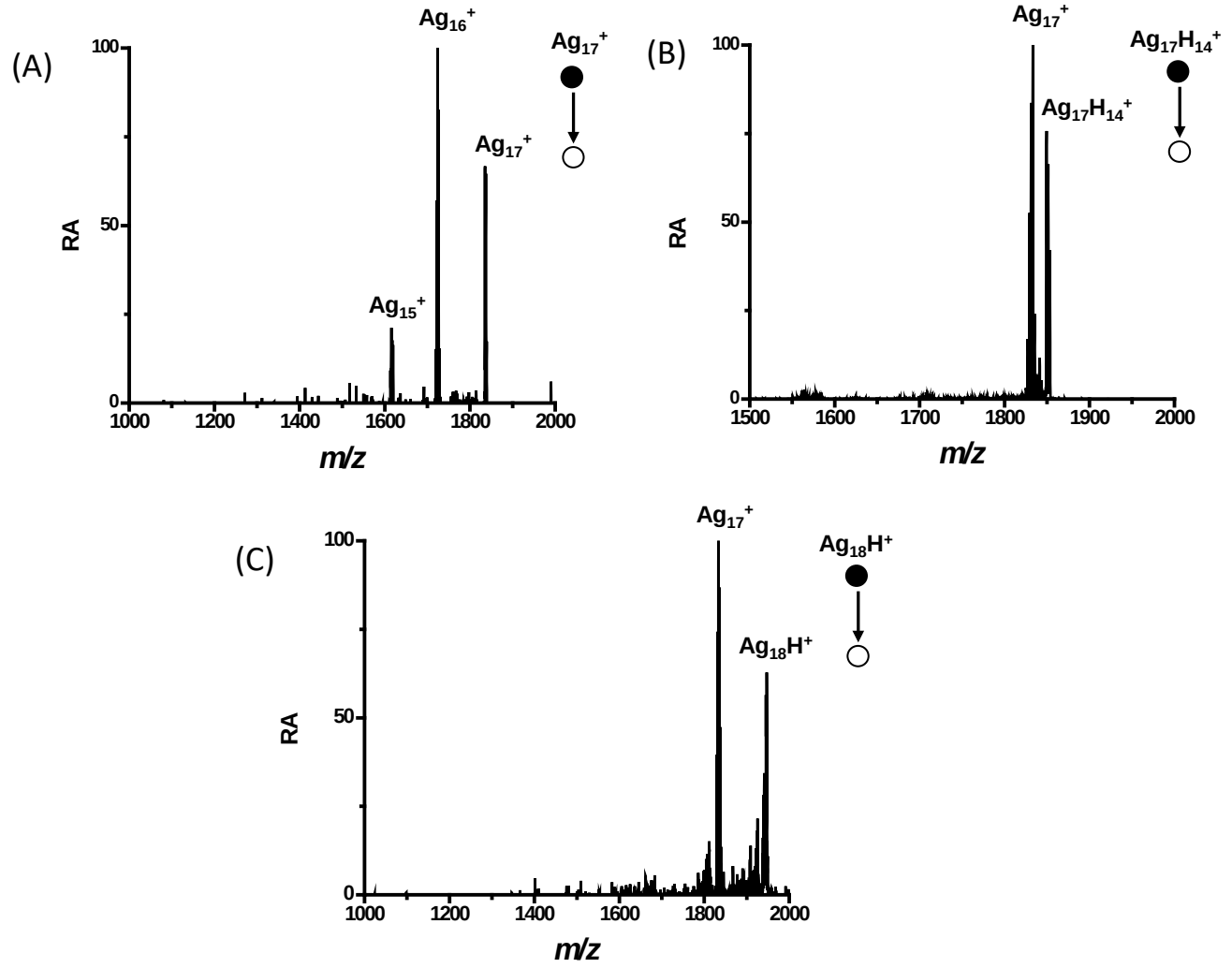


**Fig. S10** $MS^2$ for (A) $Ag_{17}^+$, (B) $Ag_{17}H_{14}^+$, (C) $Ag_{18}H^+$ ions and the isolation widths are m/z 10, 10 and 8, respectively centered at the middle of the isotopic clusters. The collision energies used for the $Ag_{17}^+$, $Ag_{17}H_{14}^+$ and $Ag_{18}H^+$ ions are 37, 17 and 24 in instrumental units, respectively. Due to higher collision energy, $Ag_{17}^+$ breaks into smaller sized naked clusters whereas the hydrides of silver ions give back the metallic core, $Ag_{17}^+$. RA refers to relative abundance.

**Supporting information 11**

**Thermal dissociation of thiolate protected cluster with the same experimental conditions:**

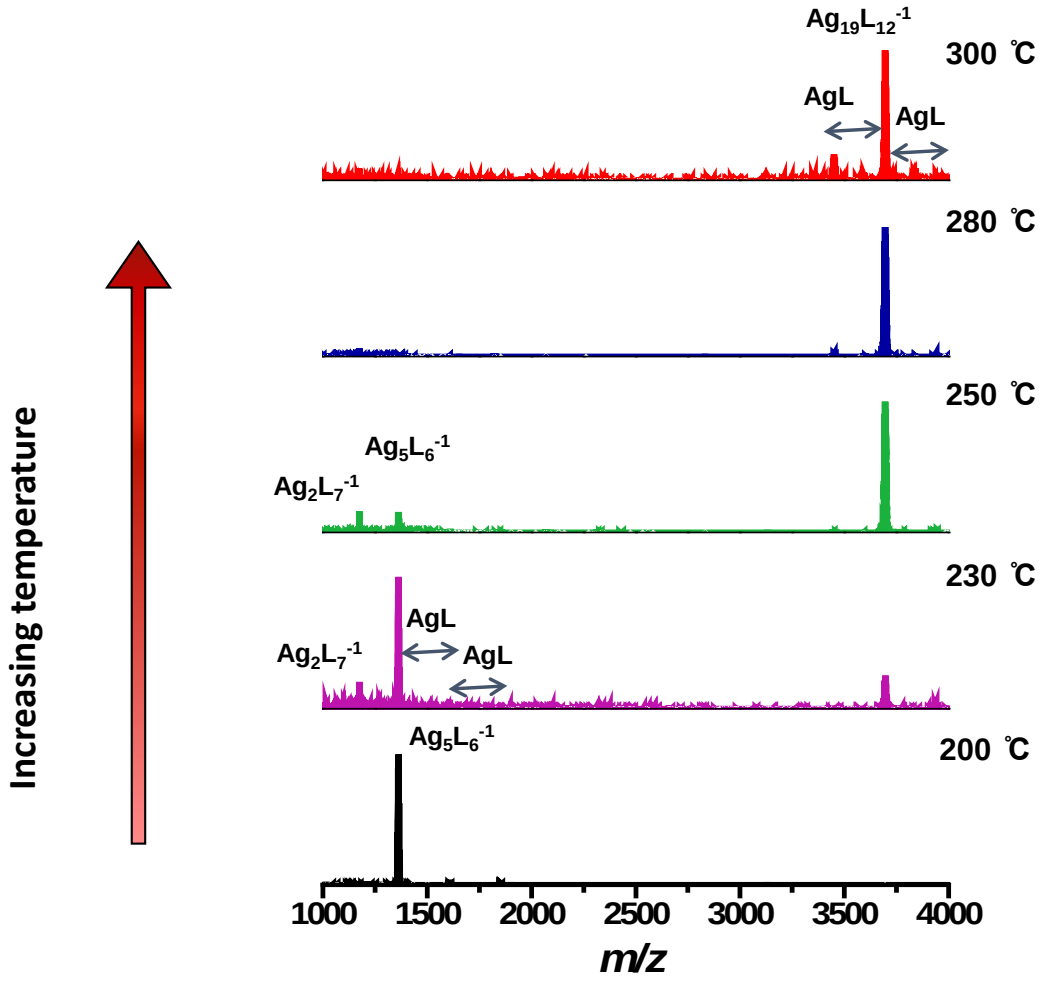


**Fig. S11** ESI mass spectra of $[Ag_{25}(DMBT)_{18}]^{3-}$ cluster at different temperatures (same conditions like before) after electrospraying the cluster solution. The thermal dissociation results in $[Ag_mL_n]^{-1}$ but not the naked cluster. Note that these clusters are thiolate protected, for them the mass spectra show intense features till the mass limit of the instrument (m/z 4000).

**Supporting information 12**

**Effect of distance between the heating tube and the ESI source:**

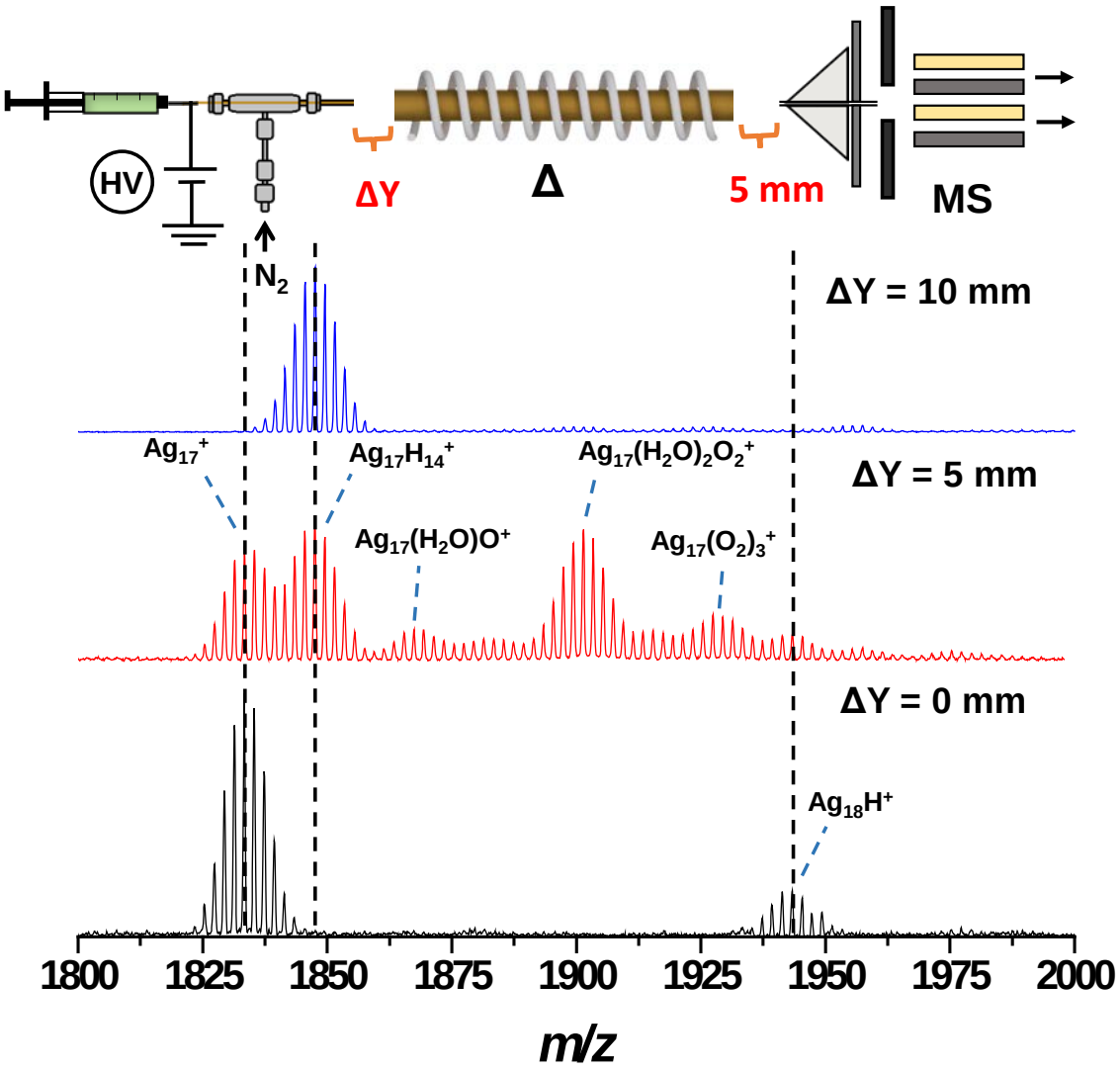


**Fig. S12** ESI mass spectra of $Ag_{17}^+$ with varying distances (ΔY) between the heating tube and ESI source keeping the constant 5 mm distance between the heating tube and inlet. Here, with increasing ΔY, $H_2O$ and $O_2$ addition peaks of $Ag_{17}^+$ appear along with the $Ag_{17}H_{14}^+$ peak. At last, only $Ag_{17}H_{14}^+$ peak appears due to the decreasing temperature, as more air flows through the heating tube.

**Supporting information 13**

## Photograph of the instrumental set-up and diagram used for ion/molecule reactions:

**(A)**

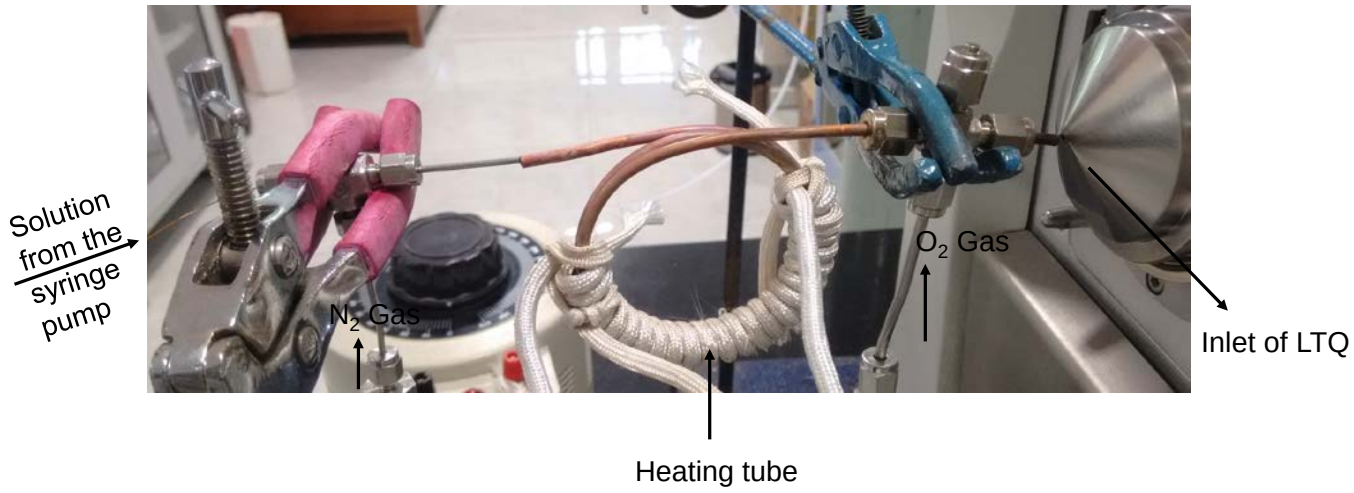


**(B)**

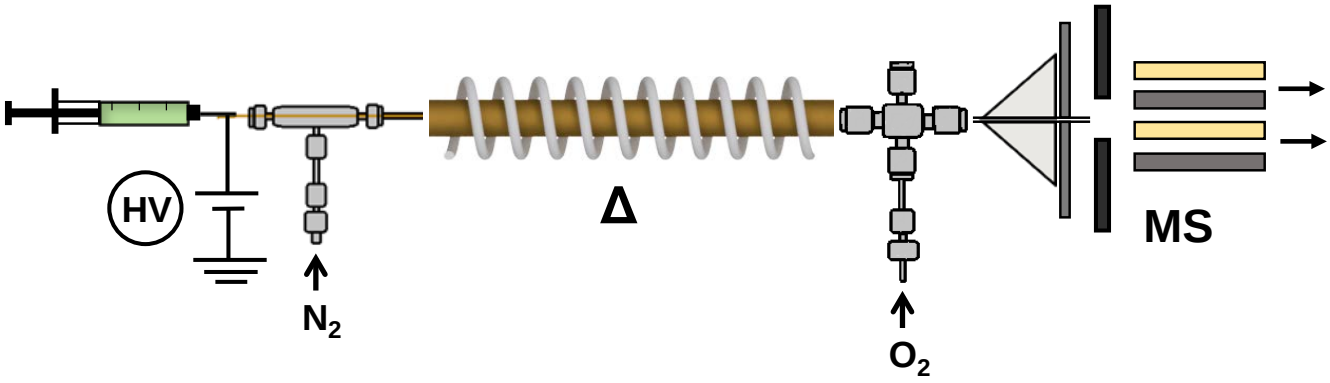


**S13:** (A) Photograph and (B) schematic diagram of the instrumental set-up used for ion/molecule reactions of naked cluster ions with oxygen.

**Supporting information 14**

## Comparison of oxygen addition reaction of naked clusters with $CD_3OD$ as solvent:

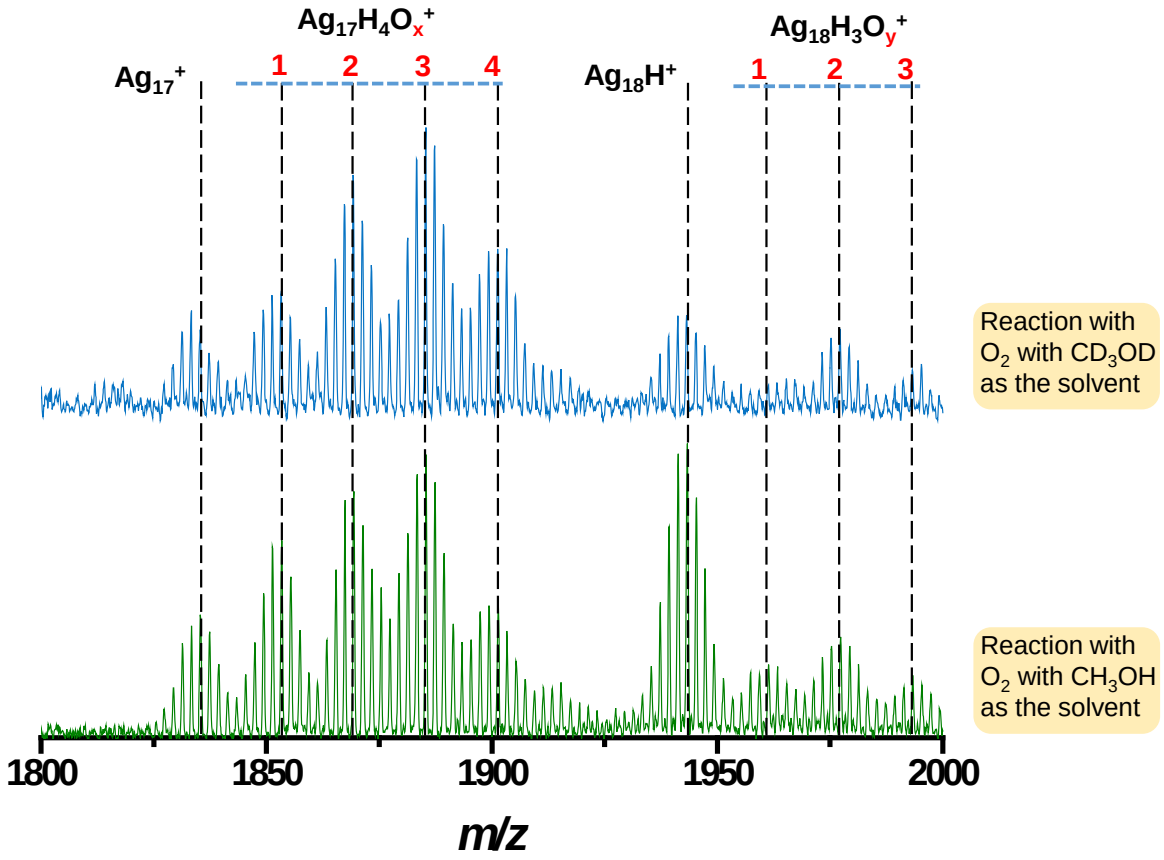


**Fig. S14** ESI mass spectra of $Ag_{17}^+$ and $Ag_{18}H^+$ ion clusters after reaction with oxygen ($O_2$) gas in presence of $CD_3OD$ and $CH_3OH$ as the two different solvents. There were no shifts for the $Ag_{17}H_4O_x^+$ and $Ag_{18}H_3O_y^+$ peaks in the case of deuterated and non-deuterated methanol as the solvents.

**Supporting information 15**

## Comparison of oxygen addition reaction of naked clusters created from $[Ag_{18}H_{16}(TPP)_{10}]^{2+}$ and $[Ag_{18}D_{16}(TPP)_{10}]^{2+}$:

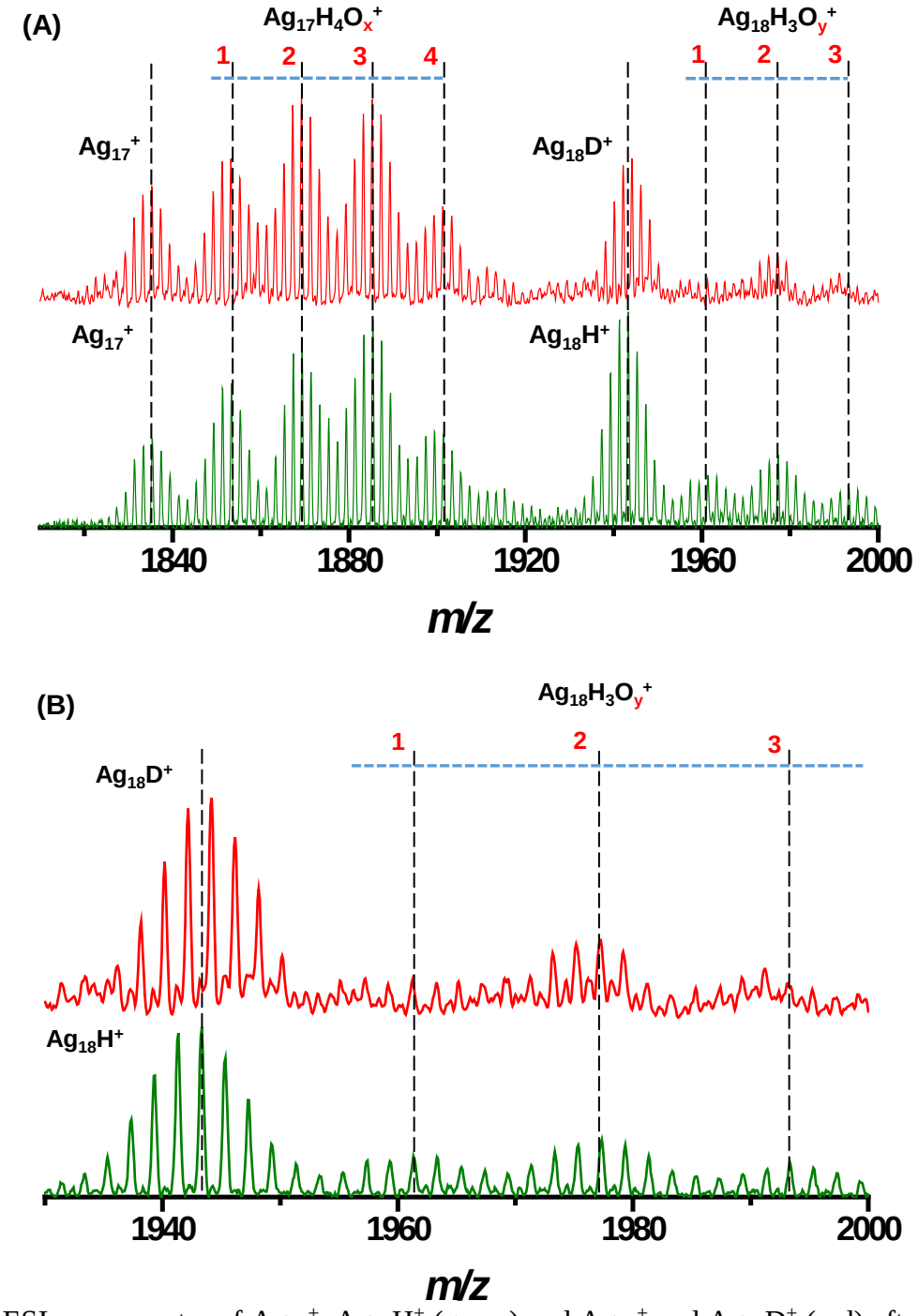


**Fig. S15** (A) ESI mass spectra of $Ag_{17}^+$, $Ag_{18}H^+$ (green) and $Ag_{17}^+$ and $Ag_{18}D^+$ (red) after reaction with oxygen ($O_2$) gas. (B) Magnified view of the isotopic separation of $Ag_{18}H_3O_y^+$, generated from both $Ag_{18}H^+$ (green) and $Ag_{18}D^+$ (red). Top and bottom spectra in each case were generated from $[Ag_{18}D_{16}(TPP)_{10}]^{2+}$ and $[Ag_{18}H_{16}(TPP)_{10}]^{2+}$, respectively. MS/MS of oxygen added peaks of $Ag_{18}H/D^+$ could not be performed due to poor intensity.

**Supporting information 16**

**Comparison of reactivity between $Ag_{17}^{+}$ and $Ag_{18}H^{+}$ ions with oxygen:**

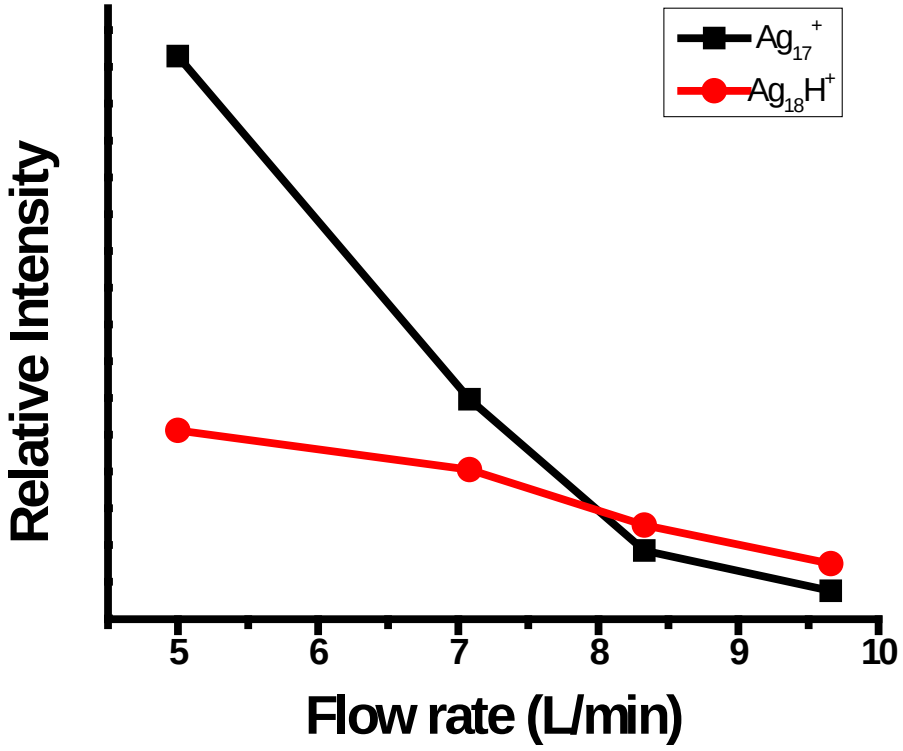


**Fig. S16** Relative intensities of $Ag_{17}^{+}$ and $Ag_{18}H^{+}$ as function of oxygen flow rate which shows the faster reactivity of $Ag_{17}^{+}$ with oxygen compared to the $Ag_{18}H^{+}$.

**Supporting information 17**

## $MS^2$ of $Ag_{17}H_4O^+$, $Ag_{17}H_4O_2^+$, $Ag_{17}H_4O_3^+$ and $Ag_{17}H_4O_4^+$ ions:

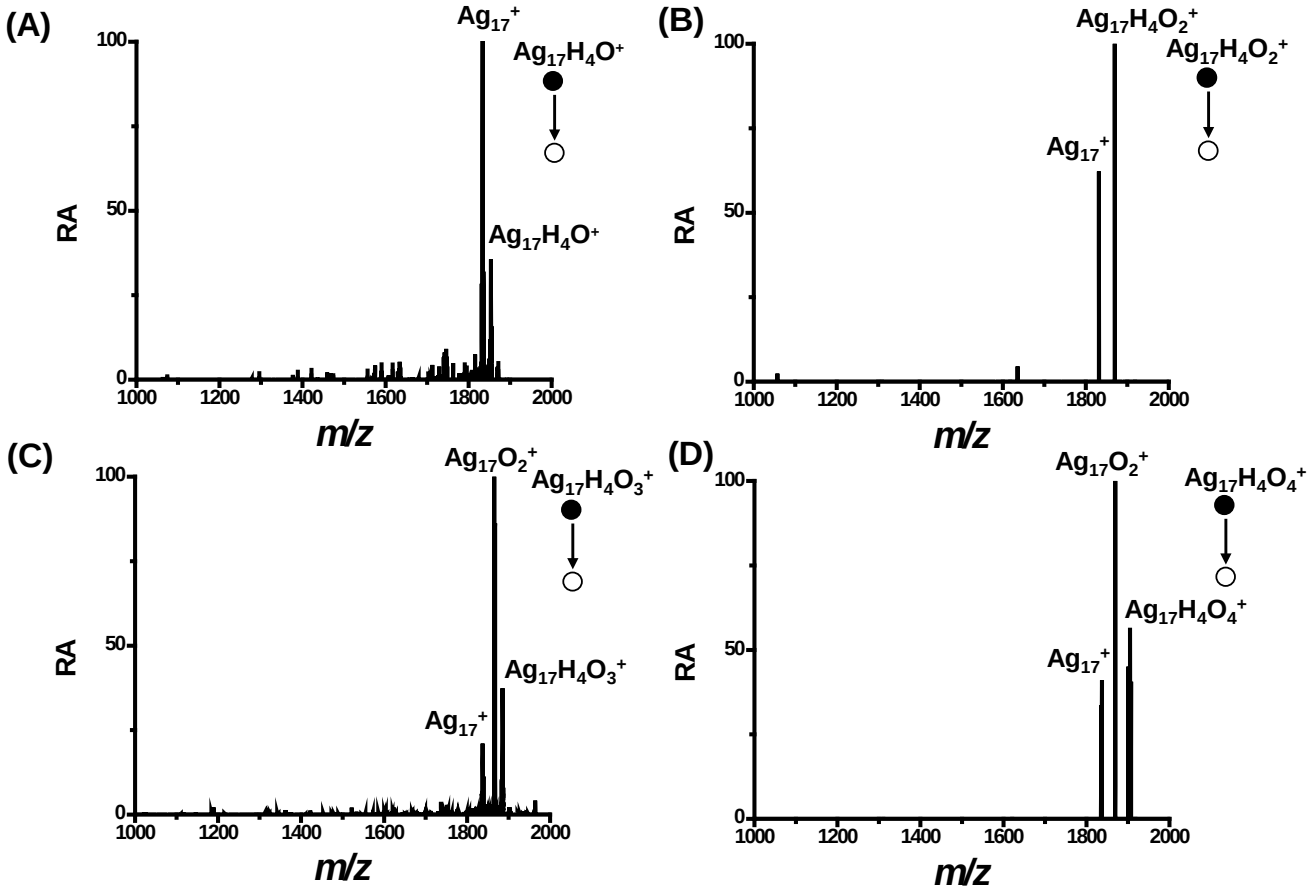


**Fig. S17** $MS^2$ of (A) $Ag_{17}H_4O^+$, (B) $Ag_{17}H_4O_2^+$, (C) $Ag_{17}H_4O_3^+$ and (D) $Ag_{17}H_4O_4^+$ and the isolation widths are m/z 5, 4.5, 4 and 3, respectively centered at the middle of the isotopic clusters. The collision energies used for $Ag_{17}H_4O^+$, $Ag_{17}H_4O_2^+$, $Ag_{17}H_4O_3^+$ and $Ag_{17}H_4O_4^+$ are 28, 50, 28 and 50 in instrumental units, respectively. For all these cases, due to collisional activation, there is oxygen detachment which results in the parent $Ag_{17}^+$ cluster. RA refers to relative abundance.

## Supporting information 18

## Comparison of $MS^2$ results of $Ag_{17}(H_2O)_2O_2^+$ and $Ag_{17}H_4O_4^+$ ions:

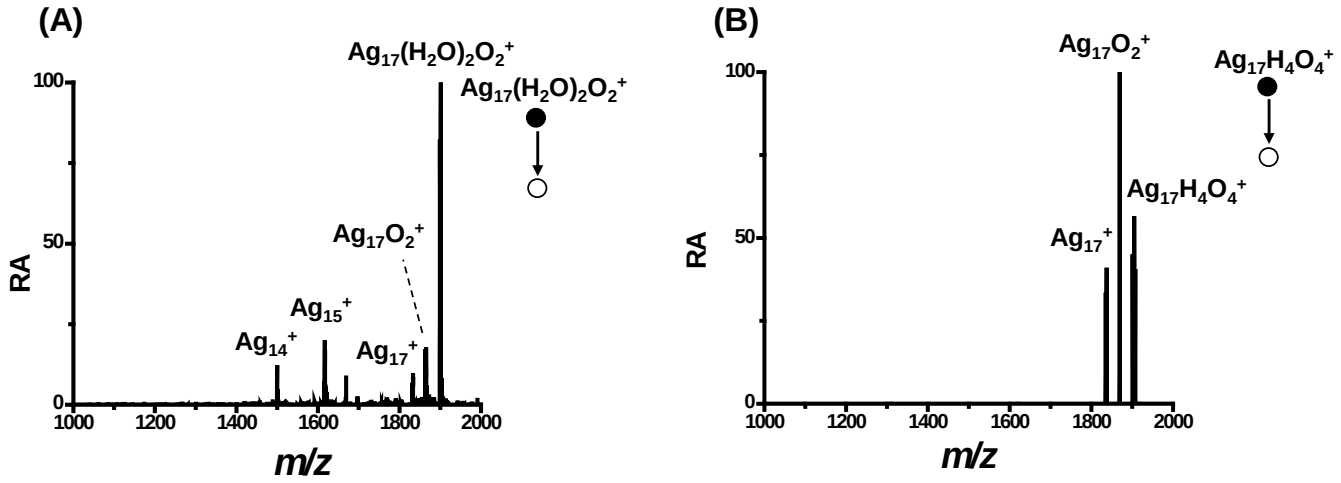


**Fig. S18** $MS^2$ spectra of (A) $Ag_{17}(H_2O)_2O_2^+$ and (B) $Ag_{17}H_4O_4^+$ at the collision energy of 50 in instrumental units. The isolation widths were m/z 5 and 3, respectively centered at the middle of the isotopic clusters. RA refers to relative abundance.

## Supporting information 19

## TEM images of $[Ag_{18}H_{16}(TPP)_{10}]^{2+}$ cluster and the electrosprayed products collected:

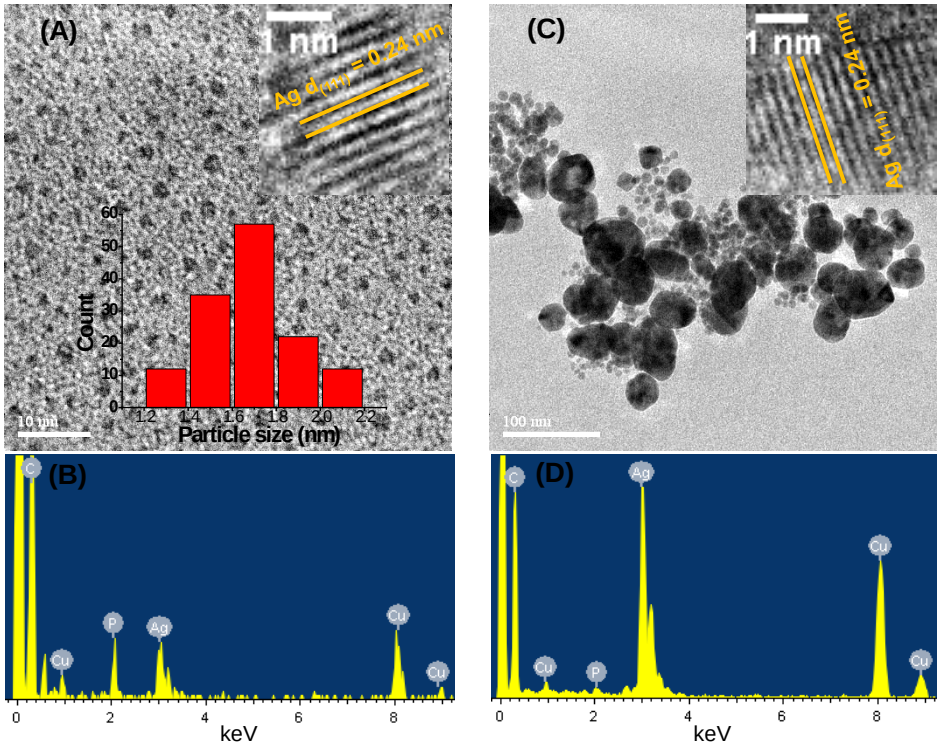


**Fig. 19** (A) TEM image of $[Ag_{18}H_{16}(TPP)_{10}]^{2+}$ cluster before electrospray. Particle distribution shows an average size of 1.68 ± 0.19 nm for the nanoclusters. Lattice spacing of 0.24 nm of $d_{(111)}$ of plane of silver is marked in the inset. (B) EDS spectrum of cluster confirms the composition. (C) TEM image of the collected electrosprayed product of $[Ag_{18}H_{16}(TPP)_{10}]^{2+}$ cluster at the heating tube temperature of 350℃. In inset, lattice spacing of 0.24 nm is marked which confirmed the $d_{(111)}$ plane of silver. (D) EDS spectrum of the collected product at heating tube temperature of 350℃.

The products of electrospray were collected using a set-up as shown below.

**Supporting information 20**

## The calculated structures of $Ag_{15}^+$, $Ag_{17}^+$, $Ag_{18}^+$, and $Ag_{18}H^+$ ions:

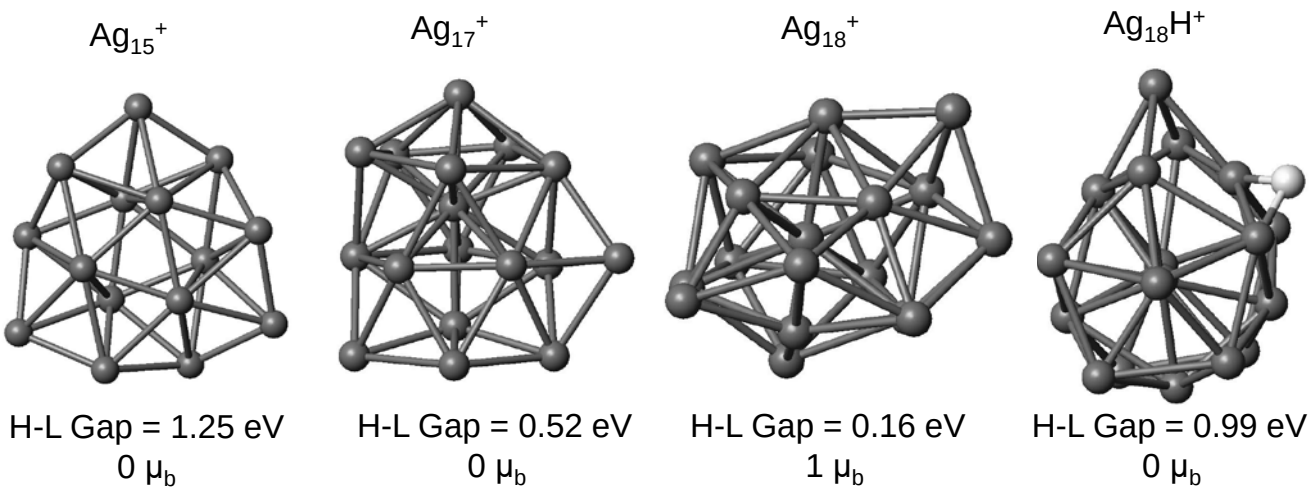


**Fig. S20** The structure and HOMO- LUMO gaps of $Ag_{15}^+$, $Ag_{17}^+$, $Ag_{18}^+$ and $Ag_{18}H^+$. $Ag_{15}^+$ was found to be resistant to $O_2$ etching due to very high HOMO-LUMO gap.

**Supporting information 21**

## Isomers of $Ag_{18}H^+$ and their energies:

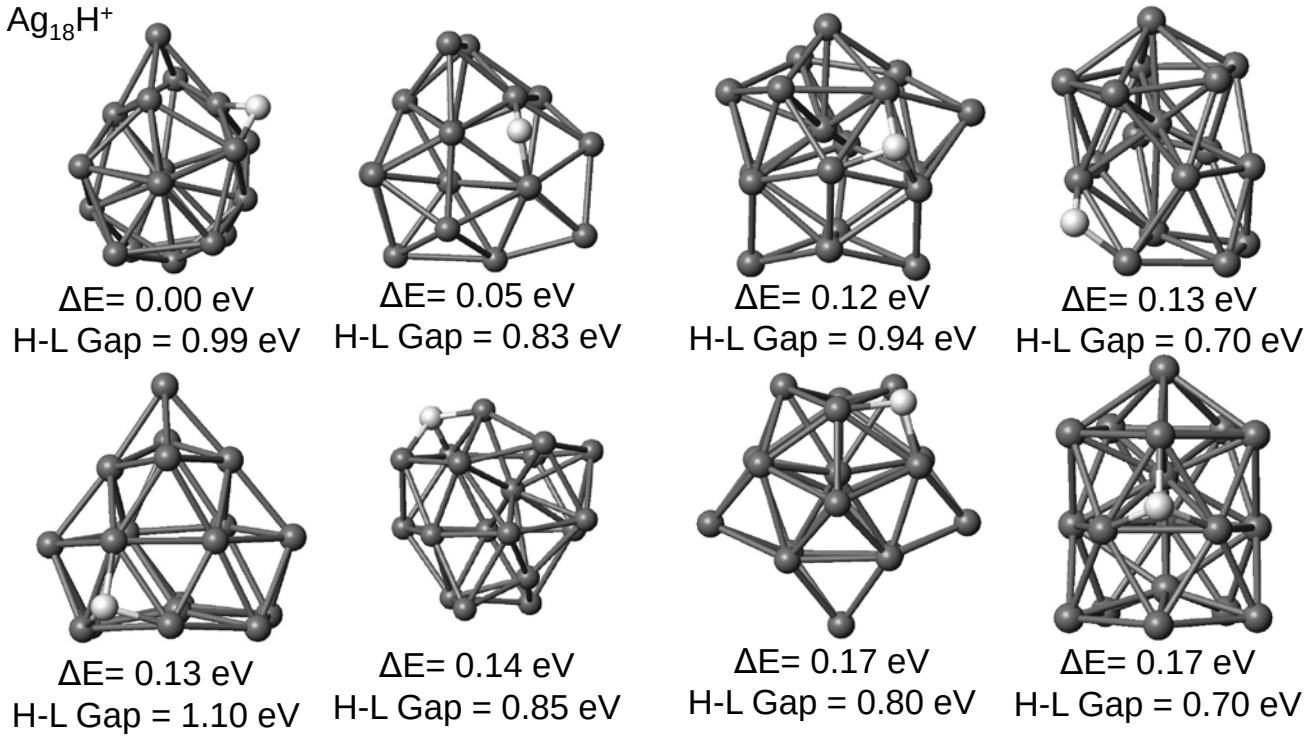


**Fig. S21** The structures, relative energies and HOMO-LUMO gaps of the lowest energy isomers for $Ag_{18}H^+$.

**Table S22**
**Experimental and calculated masses measured with the LTQ:**
The most abundant peak of the isotopic cluster is used to define the m/z value.

| Experimental m/z | Calculated m/z | Assignment $[Ag_m(PPh_3)_n(PPh_2)_oH_pO_q(H_2O)_r]^{z+}$ | | | | | | |
|---|---|---|---|---|---|---|---|---|
| | | Ag (m) | $PPh_3$ (n) | $PPh_2$ (o) | H (p) | O (q) | $H_2O$ (r) | Charge (z) |
| 183.00 | 182.95 | | | 1* | | | | 1 |
| 262.17 | 262.09 | | 1 | | | | | 1 |
| 294.08 | 294.08 | | 1 | | | 2 | | 1 |
| 297.17 | 297.10 | | 1 | | 1 | 1 | 1 | 1 |
| 386.83 | 387.01 | 1 | 1 | | 2 | 1 | | 1 |
| 400.83 | 400.99 | 1 | 1 | | | 2 | | 1 |
| 631.17 | 631.09 | 1 | 2 | | | | | 1 |
| 647.17 | 647.08 | 1 | 2 | | | 1 | | 1 |
| 1185.92 | 1185.95 | 11 | | | | | | 1 |
| 1294.75 | 1294.86 | 12 | | | | | | 1 |
| 1401.67 | 1401.76 | 13 | | | | | | 1 |
| 1454.08 | 1454.09 | 11 | 1 | | 6 | | | 1 |
| 1510.50 | 1510.67 | 14 | | | | | | 1 |
| 1521.67 | 1521.75 | 14 | | | 10 | | | 1 |
| 1617.42 | 1617.57 | 15 | | | | | | 1 |
| 1726.33 | 1726.48 | 16 | | | | | | 1 |
| 1737.58 | 1737.56 | 16 | | | 11 | | | 1 |
| 1833.42 | 1833.38 | 17 | | | | | | 1 |
| 1847.50 | 1847.49 | 17 | | | 14 | | | 1 |
| 1853.42 | 1853.41 | 17 | | | 4 | 1 | | 1 |
| 1867.33 | 1867.39 | 17 | | | | 1 | 1 | 1 |
| 1869.42 | 1869.40 | 17 | | | 4 | 2 | | 1 |
| 1885.33 | 1885.40 | 17 | | | 4 | 3 | | 1 |
| 1901.33 | 1901.39 | 17 | | | | 2 | 2 | 1 |
| 1901.42 | 1901.39 | 17 | | | 4 | 4 | | 1 |
| 1929.33 | 1929.35 | 17 | | | | 6 | | 1 |
| 1943.42 | 1943.30 | 18 | | | 1 | | | 1 |
| 1955.50 | 1955.39 | 18 | | | 13 | | | 1 |
| 1961.25 | 1961.31 | 18 | | | 3 | 1 | | 1 |
| 1977.33 | 1977.30 | 18 | | | 3 | 2 | | 1 |
| 1993.33 | 1993.30 | 18 | | | 3 | 3 | | 1 |

*Peak is seen with two hydrogens losses.

**Table S23**
**Experimental and calculated masses measured using the G2-Si:**
The most abundant peak of the isotopic cluster is used to define the m/z value.

| Experimental m/z | Calculated m/z | Assignment $[Ag_m(PPh_3)_nH_o]^{z+}$ | | | |
|---|---|---|---|---|---|
| | | Ag (m) | $PPh_3$ (n) | H (o) | Charge (z) |
| 2290.1587 | 2290.2152 | 18 | 10 | 16 | 2 |
| 2159.3291 | 2159.6199 | 18 | 9 | 16 | 2 |
| 2028.3219 | 2028.5740 | 18 | 8 | 16 | 2 |
| 1897.3425 | 1897.5281 | 18 | 7 | 16 | 2 |
| 1765.8406 | 1765.9827 | 18 | 6 | 16 | 2 |